catalysts

MDPI

Article

Activated Carbon-Loaded Titanium Dioxide Nanoparticles and Their Photocatalytic and Antibacterial Investigations

Chelliah Parvathiraja [1,*], Snehlata Katheria [2], Masoom Raza Siddiqui [3], Saikh Mohammad Wabaidur [3], Md Ataul Islam [4] and Wen-Cheng Lai [5,6,*]

1 Department of Physics, Manonmaniam Sundaranar University, Tirunelveli 627012, Tamilnadu, India
2 Chemistry Department, Lucknow University, Lucknow 226007, Uttar Pradesh, India; snehakhtr2208@gmail.com
3 Chemistry Department, College of Science, King Saud University, Riyadh 11451, Saudi Arabia; siddiqui124@gmail.com (M.R.S.); swabaidur@ksu.edu.sa (S.M.W.)
4 Division of Pharmacy and Optometry, School of Health Sciences, Faculty of Biology, Medicine and Health, University of Manchester, Manchester M13 9PL, UK; ataul.islam80@gmail.com
5 Bachelor Program in Industrial Projects, National Yunlin University of Science and Technology, Douliu 640301, Taiwan
6 Department of Electronic Engineering, National Yunlin University of Science and Technology, Douliu 640301, Taiwan
* Correspondence: cpraja1206@gmail.com (C.P.); wenlai@yuntech.edu.tw or wenlai@mail.ntust.edu.tw (W.-C.L.)

Abstract: Activated carbon doping TiO_2 nanoparticles were synthesised by zapota leaf extract using the co-precipitation method. The bio-constituents of plant compounds were used in the reactions of stabilization and reductions. The carbon loading on the TiO_2 nanoparticles was characterised by XRD, FTIR, UV-DRS, SEM with EDX, and TEM analysis. The loading of activated carbon onto the TiO_2 nanoparticles decreased the crystallite size and optical bandgap, and their doping improved the surface structure of AC/TiO_2 nanoparticles. Mesoporous/microporous instability was remodified from the activated carbon, which was visualised using SEM and TEM analysis, respectively. The photocatalytic dye degradation of Rh-B dye was degraded in TiO_2 and AC/TiO_2 nanoparticles under visible light irradiation. The degradation efficiencies of TiO_2 and AC/TiO_2 nanoparticles were 73% and 91%, respectively. The bacterial abilities of TiO_2 and AC/TiO_2 nanoparticles were examined by *E. coli* and *S. aureus*. The water reclamation efficiency and bactericidal effect of TiO_2 and AC/TiO_2 nanoparticles were examined via catalytic dye degradation and bacterial efficiency of activated carbon-doped titanium dioxide nanoparticles.

Keywords: TiO_2 and AC/TiO_2 nanoparticles; photocatalysis; antibacterial activity; Rh-B; zapota leaf; bio-synthesis

Citation: Parvathiraja, C.; Katheria, S.; Siddiqui, M.R.; Wabaidur, S.M.; Islam, M.A.; Lai, W.-C. Activated Carbon-Loaded Titanium Dioxide Nanoparticles and Their Photocatalytic and Antibacterial Investigations. *Catalysts* **2022**, *12*, 834. https://doi.org/10.3390/catal12080834

Academic Editor: Damian C. Onwudiwe

Received: 4 June 2022
Accepted: 27 July 2022
Published: 29 July 2022

1. Introduction

Water scarcity is an important and big issue in the current world. The demand for water is influenced by the development of industries and population increments [1–6]. Technology and population growth affect water bodies through various associated compounds. Dyes, germs, chemicals, and parasites are among the components that are integrated into water bodies and changed to unpleasant and non-drinkable water. Dyes, chemicals, microbes, and parasites are among the components that are integrated into water bodies and changed into unpleasant and non-drinkable water [7–10]. Among the pollutants, organic and biological compounds are very toxic to living organisms. Inadequacies in the water system have been remedied through the application of nanomaterials for either wastewater treatment or water reuse systems. Numerous technologies are elaborate in the water reclamation process, such as filtrations, coagulations, adsorption, and photocatalysts [11,12]. The photocatalyst method is an efficient technique and more powerful and convenient than other remediation processes. In addition, the photocatalyst remediation process derives non-toxic compounds,

and their by-products are noxious-free compounds. Metal oxides as photocatalysts facilitate the maximum and more resourceful applications than metal photocatalysts due to their wide bandgap and their recombination of photo charge carriers [13–16]. TiO_2, ZnO, and CeO_2 metal oxides containing the 3.2 eV bandgap are the same, but TiO_2 possesses a larger surface area and higher oxidization ability than other metal oxides [17–20]. Hence, the phase formation of TiO_2 nanoparticles and their short response in visible light and rapid recombination are major drawbacks of TiO_2 nanoparticles. These drawbacks can be circumvented and eliminated by using carbon decoration/doping on the TiO_2 nanoparticles. Carbon-based materials possess a large number of applications in various fields due to their large surface area and porous nature [15–21]. Diamond, graphene, fullerene, activated carbon, and coal are all examples of carbon allotropes. Carbon in various forms can be utilised in supercapacitors, energy storage devices, and photocatalysts due to their long-term stability, chemical compatibility, and chemical and mechanical qualities [16–18]. Among the carbon allotropes, activated carbon has a unique nature because it emanates a double layer of surface area on the coating material and has high porosity compared to other carbon forms. These properties are highly appreciated in adsorption activity in water and gas separation developments. The porosity nature is classified into three phases, (i) mesoporous, (ii) microporous, and (iii) macroporous [19–21]. Activated carbon has mesoporous and microporous attitudes that absorb big and small molecules from the surface. The large liquid molecules are adsorbed by activated carbon in mesoporous form, and small gas molecules are captured from the microporous state [22–24]. The ratio between mesoporous and microporous is a very important condition to form an efficient adequate activated carbon system. Activated carbon is synthesised from bio-waste and a greenway production process, which is a highly eco-friendly synthesis method [25–30]. The present work aimed to remove water pollution through activated carbon-doped TiO_2 nanoparticles. Three important developments are discussed in the current work: (i) visible light adsorption is enhanced using activated carbon to dope the TiO_2 lattice; (ii) recombination processes are extended by using activated carbon; and (iii) mesoporous and microporous ratios are maintained by using TiO_2 nanoparticles. These frames of action extensively degraded and adsorbed the organic pollutants and bacterial activities.

2. Materials and Methods

2.1. Materials

All the chemicals were procured from Merck India. The reductant of Manilkara zapota leaf was collected from Tamilnadu, India. Synthesised chemicals of activated carbon and titanium tetra isopropoxide (TTIP) were used at an analytical grade (AR). Double distilled water was used for further synthesis, and extra modifications did not occur in the synthesised process.

2.2. Manilkara Zapota Leaf Extract Preparation

A total of 500 mg of fresh Manilkara zapota leaf was collected from a garden. The obtained leaves were washed with tap water, rinsed with double distilled water, and then dried at room temperature for 6 h. Finally, dried samples were mixed with 200 mL of double distilled water and heated to 100 °C for 60 min. The boiled extract was filtered by Whatman No.1 filter paper and stored for further synthesis processes.

2.3. Synthesis of TiO_2 Nanoparticles

The 1 M TTIP solution was dissolved in 90 mL of double distilled water and mixed with 10 mL of plant extract. The mixed solution was stirred for 6 h, and the temperature was maintained at 60 °C. Ti compounds slowly reduced their colour configuration to a milk-white colour formation. After stirring the colour-reduced solution, it was centrifuged for 10,000 rpm for 180 s, and this was repeated three times to eliminate unwanted compounds from the surface. Then, the precipitate was processed using double distilled water and

dried at 80 °C for one day. Finally, the obtained nanophase powder was stored for further characterizations.

2.4. Preparation of AC/TiO_2 Nanoparticles

An amount of 2 g of the activated carbon source was poured into a 1 M TTIP solution and 10 mL of plant extract. The combined source solution was stirred for 6 h at 60 °C, which produced the precipitate form of AC/TiO_2 nanoparticles. The nano precipitate was purified from the centrifugation process for 10,000 rpm at 180 s (3 times) and washed with double distilled water. The purified precipitate obtained after removing the supernatant was kept in an oven at 800 °C for 24 h. The final AC/TiO_2 nanoparticles were stored for further measurements.

2.5. Characterization of AC/TiO_2 Nanoparticles

The phase details and structural information were monitored from X-ray diffraction (XRD-PANalytical B.V., Overijssel, The Netherlands). The chemical compounds and their functionality compounds and groups were captured from Fourier transform infrared (FT-IR-Perkin Elmer, Waltham, MA, USA). The optical imperfections and their electronic mitigations were recorded using UV-DRS (UV-2700, Shimadzu, Kyoto, Japan) analysis. The surface morphology and their modifications of the synthesised nanoparticles were derived from transmission electron microscopy (TEM-FEI Titan 80–300, Bangalore, India), and scanning electron microscopy (SEM-Carl Zeiss, Jena, Germany) coupled with EDAX spectroscopy measured the elemental presence of the nanoparticles. Binding energy and their bonding were measured from XPS (Physical Electronics Model-PHI 5000 Versa Probe III-Chanhassen, MN, USA)

2.6. Bacterial Suspension

The antibacterial activity was determined using *Escherichia coli* 745 and *Staphylococcus aureus* 9779 as bacterial sources. Layreint Broth (LB) medium was used to prepare the Gram-positive *S. aureus* and Gram-negative bacteria *E. coli* under the conditions of 36 °C/48 h. The well diffusion method helped to determine the bacterial efficacy of synthesised nanoparticles. The well wall was created using a cork borer, and its diameter was 0.85 cm on the Petri plates. The different concentrations (10, 25, 50, and 100 µL) of the nanoparticles sample were loaded into the created well and incubated for 24 h at 36 °C. The bacterial growth rate was calculated using the zone of inhibitions, and the range was measured in millimetres.

2.7. Photocatalytic Degradation Experiment

The visible light photocatalytic dye degradation of Rh-B dye was treated under solar irradiation. The 10 mL (dye concentration was 1×10^{-5} M) Rh-B solution was dissolved in 10 mg of nanoparticles and placed in a dark condition to reach the equilibrium positions. After that, the mixed solution was irradiated by solar light with continuous stirring. At 5 min, the aliquot was taken out and centrifuged to remove the nanoparticles, and the degradation efficiency was measured by the following formula.

$$\text{Dye removal percentage (\%)} = (C_a - C_b/C_a) \times 100$$

where

$\mathbf{C_a}$ = Initial Rh-B concentrations at time = 0.

$\mathbf{C_b}$ = Active dye concentrations at time = 5 min.

The quenching experiment helps to find the active species (superoxides, free radicals, and holes) of the photocatalyst. The 1 mmol/L concentration quenchers (triethanolamine (TEOA), p-benzoquinone (BQ), and (isopropyl alcohol (IPA)) were used in the analysis, and their measurements were captured from UV–Visible spectroscopy.

3. Results and Discussion

3.1. XRD Analysis

Figure 1 shows the X-ray diffraction pattern of titanium dioxide and activated carbon-decorated titanium dioxide nanoparticles. The pure titanium dioxide nanoparticles obtained diffractive patterns at 2θ = 25.44$^{\theta}$, 38$^{\theta}$, 47.94$^{\theta}$, 54.13$^{\theta}$, 54.81$^{\theta}$, 62.75$^{\theta}$, 69.08$^{\theta}$, 70.8$^{\theta}$, and 74.84$^{\theta}$ values, which are associated with (1 0 1), (0 0 4), (2 0 0), (1 0 5), (2 1 1), (2 0 4), (1 1 6), (2 2 0), and (2 1 5) planes, respectively. The obtained values coincided well with the anatase phase standard JCPDS card number: 89–4921 and their tetragonal structure [31,32]. The anatase phase stability is very high compared to other phases of titanium dioxide nanoparticles, which can accelerate the electron accumulations on the surfaces. The doping of activated carbon reformed the titanium dioxide nanoparticles lattice arrangement, which can be coated on the titanium dioxide surfaces. The activated carbon existence was confirmed by 2θ = 25.33$^{\theta}$ (0 0 2), which moved towards the lower wavelength side. The peak displacement on the titanium dioxide surfaces provides evidence of the formation of activated carbon doping on the surfaces. The obtained 2θ values ensured the activated carbon presence and were confirmed by the standard JCPDS card number 75–1621 [33–35]. The activated carbon increased the electron accumulations on the surface and modified the crystal regularity. The crystallite sizes of the nanoparticles were calculated using the Scherrer formula. The calculated crystallite sizes are 29 nm and 23 nm for TiO_2 and AC/TiO_2 nanoparticles, respectively. The incorporation of activated carbon increased the lattice orderings and decreased the void between atoms, which deducted the crystallite sizes. The enhanced crystallite sizes of the AC/TiO_2 nanoparticles are an efficient alternative for water remediation and biological inactivation activities.

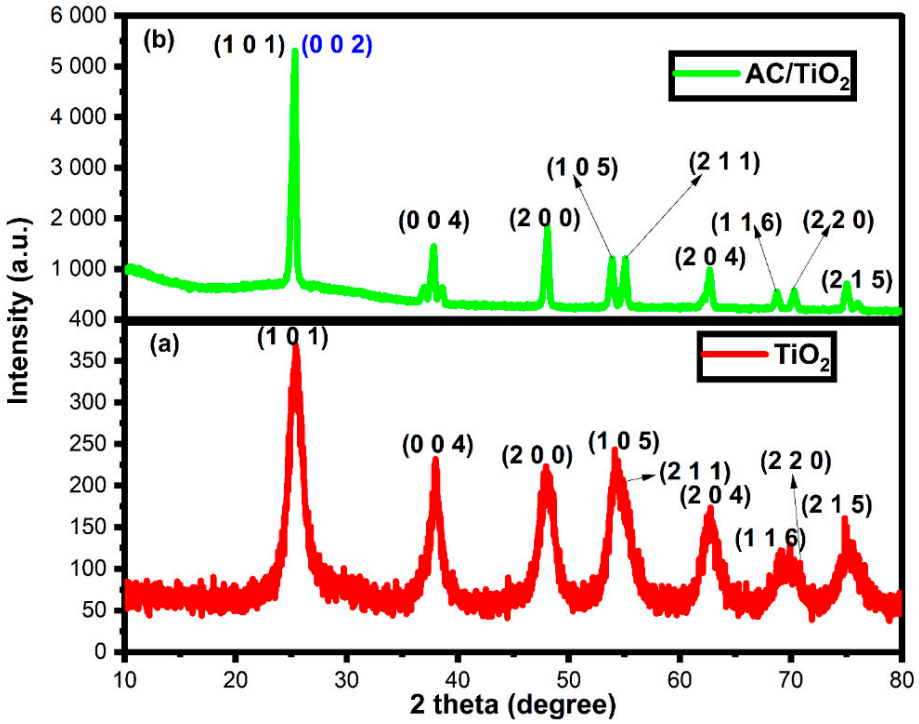

Figure 1. X-ray diffraction pattern of TiO_2 (**a**) and AC/TiO_2 (**b**) nanoparticles.

3.2. FTIR Analysis

Figure 2 displays the functional groups of the TiO_2 and AC/TiO_2 nanoparticles. The broad peak of pure TiO_2 nanoparticles located at 3238 cm^{-1} exhibited OH-stretching on the nanoparticles' surface, which absorbed the phenolic compounds, alcohols, and water molecules [36,37]. An aromatic ring vibration at the C=C stretching peak was seen at 1634 cm^{-1}, carboxylic acid formation was seen at 1524 cm^{-1}, and C-H asymmetric

stretching from the plant derivatives was exhibited at the peak of 1417 cm^{-1}, which was derived from the zapota plant extract [38–40]. The wide peak at 759 cm^{-1} and the narrow peak at 553 cm^{-1} indicated the formation of activated carbon-loaded titanium dioxide nanoparticles and established the oxygen–metal–oxygen bonding [41]. The activated carbon loading modified the adsorption capability of TiO_2 nanoparticles. The peak of 2984 cm^{-1} decreased their intensity due to the doping of activated carbon and derived the OH-stretching on the surface [42]. The 1731 cm^{-1} peak indicates the existence of amine compounds from biomolecules. The 1365 cm^{-1} peak represents the secondary amide compounds derived from phenolic plant compounds. The peak at 1218 cm^{-1} denotes the stretching vibrations of the C-O bond [43–45]. The peaks at 898 cm^{-1} and 516 cm^{-1} characterised the C-O-Ti-O bonding [46], which recognised the formation of activated carbon-loaded titanium dioxide nanoparticles. Activated carbon loading or substitution on titanium oxide nanoparticles was obtained from plant bio-molecules.

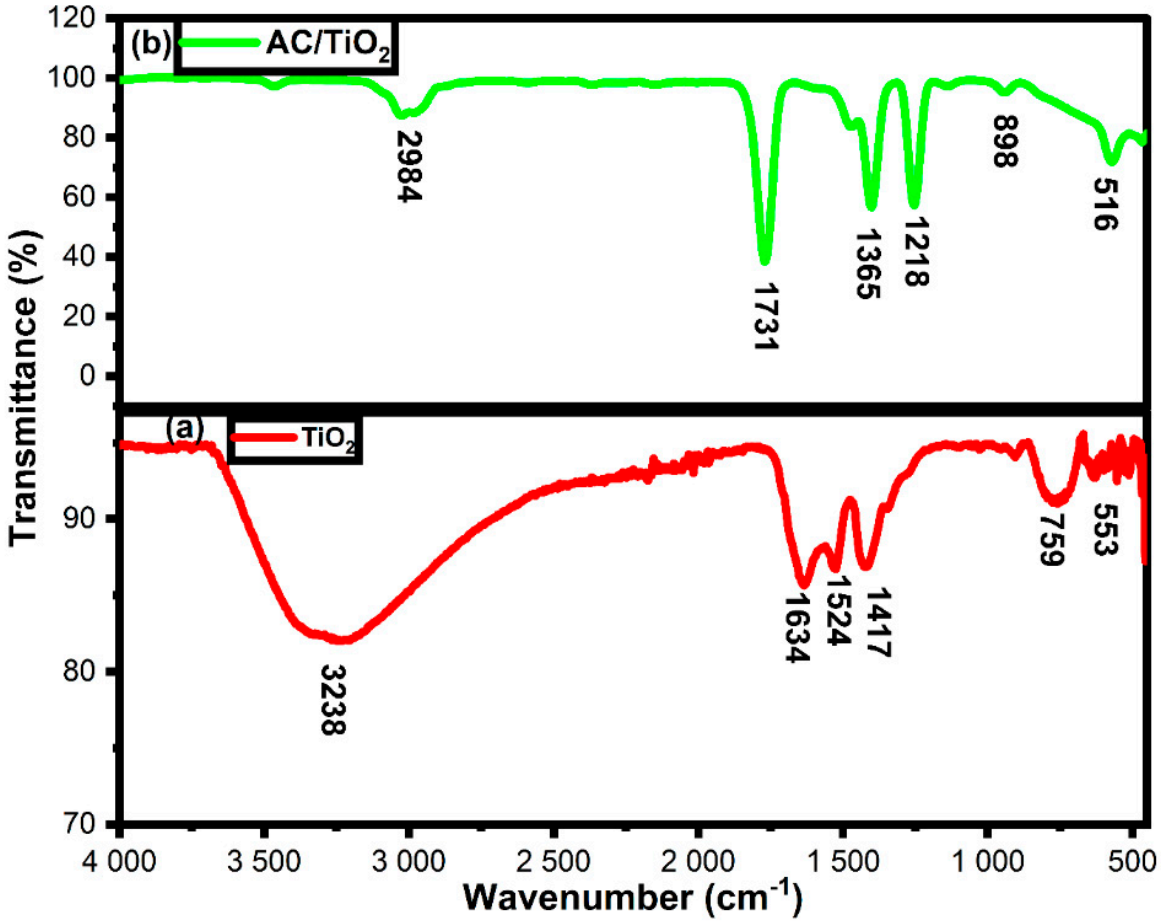

Figure 2. FTIR spectrum of TiO_2 (**a**) and AC/TiO_2 (**a**) nanoparticles.

3.3. UV-DRS Analysis

The UV-DRS measurements of synthesised TiO_2 and AC/TiO_2 nanoparticles are displayed in Figure 3. Figure 3a exposes the optical insights of the synthesised nanoparticles, and their optical limit was characterised by the ultraviolet and visible regions. The pure TiO_2 nanoparticles exhibited an absorption edge at 370–390 nm, which described the green emission of TiO_2 nanoparticles. In addition, the O-Ti-O formations of Ti^{4+} cations established the UV region absorption in TiO_2 nanoparticles. Activated carbon doping to the Ti^{4+} cations increased the electron excitations and produced a higher quantity of charge carriers than pure TiO_2 nanoparticles. When activated carbon is added to the Ti^{4+} cationic system, the peaks shift to the higher wavelength side (redshift). Furthermore, the Ti^{4+}

cations increased the adsorbing behaviour due to their modifications of crystal lattices by doping activated carbon. The optical defect and electron migrations are well constructed by calculating the bandgap of the nanoparticles. The Kubelka–Munk relations were used to find the bandgap of synthesised nanoparticles. The obtained values are demonstrated in Figure 3b. The pure anatase TiO_2 is 3.11 eV, well matched with the previous TiO_2 nanoparticle value and standard anatase bandgap of TiO_2 nanoparticles [47–51]. The wide bandgap of TiO_2 nanoparticles was modified with the activated carbon, which reduced the bandgap to 2.73 eV. The energy difference is 0.38 eV which established the visible light absorption and evidenced the production of photo-charge carriers. The generations of charge carriers increased the free radicals and enhanced the recombination activity, which provoked efficient catalytic degradation activity [52]. The radical generation promotes bactericidal activity and is highly appreciable in biomedical developments.

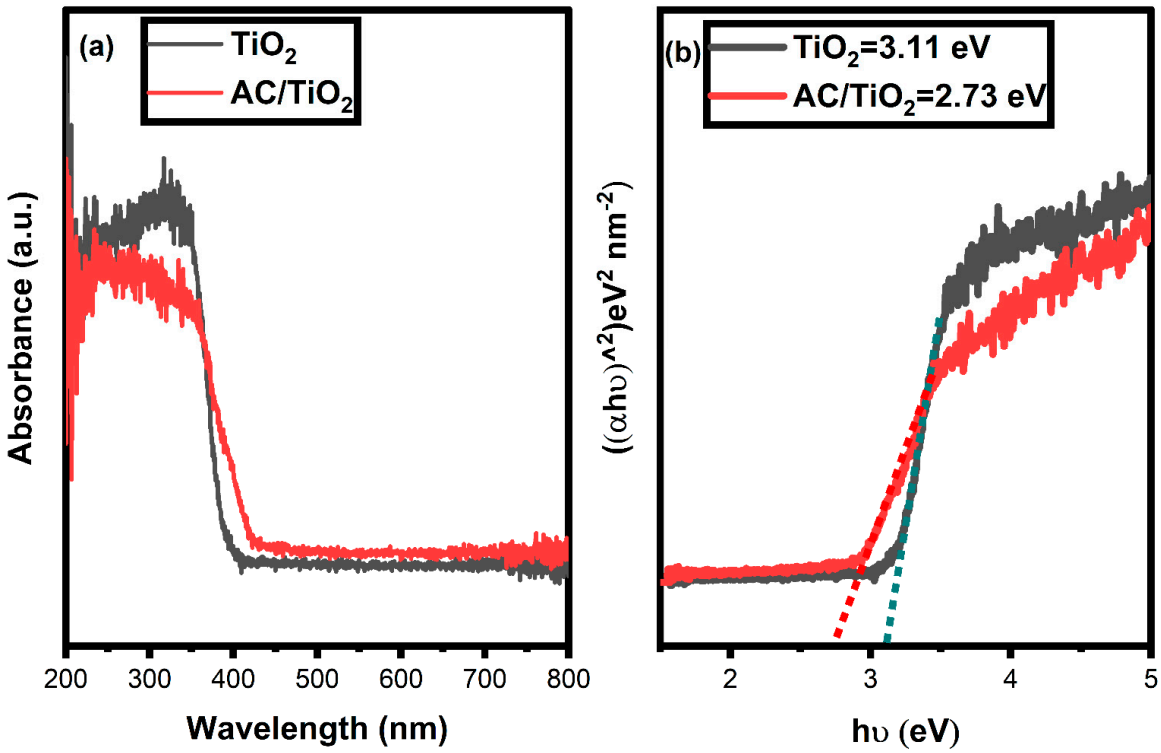

Figure 3. UV-DRS absorbance (**a**) and bandgap spectrum (**b**) of TiO_2 and AC/TiO_2 nanoparticles.

3.4. SEM with EDX and TEM Analysis

The synthesised nanoparticles' surface morphology and their elemental disorder properties were measured from SEM with EDX spectrum, as shown in Figure 4. The pure TiO_2 nanoparticles exhibited semi-spherical and spherical shapes on the surface. The semi-spherical shapes were attained from the plant molecules. The plant molecules' infringement over the surface creates a large molecule, and their existence builds semi-spherical formations of TiO_2 nanoparticles [53,54]. The distribution and spherical formations are displayed in Figure 4a,b. The addition of activated carbon to the TiO_2 nanoparticles formed an equal spherical shape and even distribution over the nanoparticles' surface, as shown in Figure 4c,d. The pure TiO_2 nanoparticles demonstrated that the particle size is 30 nm and AC/TiO_2 is 22 nm, which are close to the XRD crystallite size values. The energy dispersion on the elements was characterised by EDX spectroscopy, and their spectrum and table are presented in Figure 4e. The carbon, titanium, and oxygen elements were confirmed from the EDX peaks and table. The low amount of carbon modified the surface morphology and created a mono-dispersion over the surfaces.

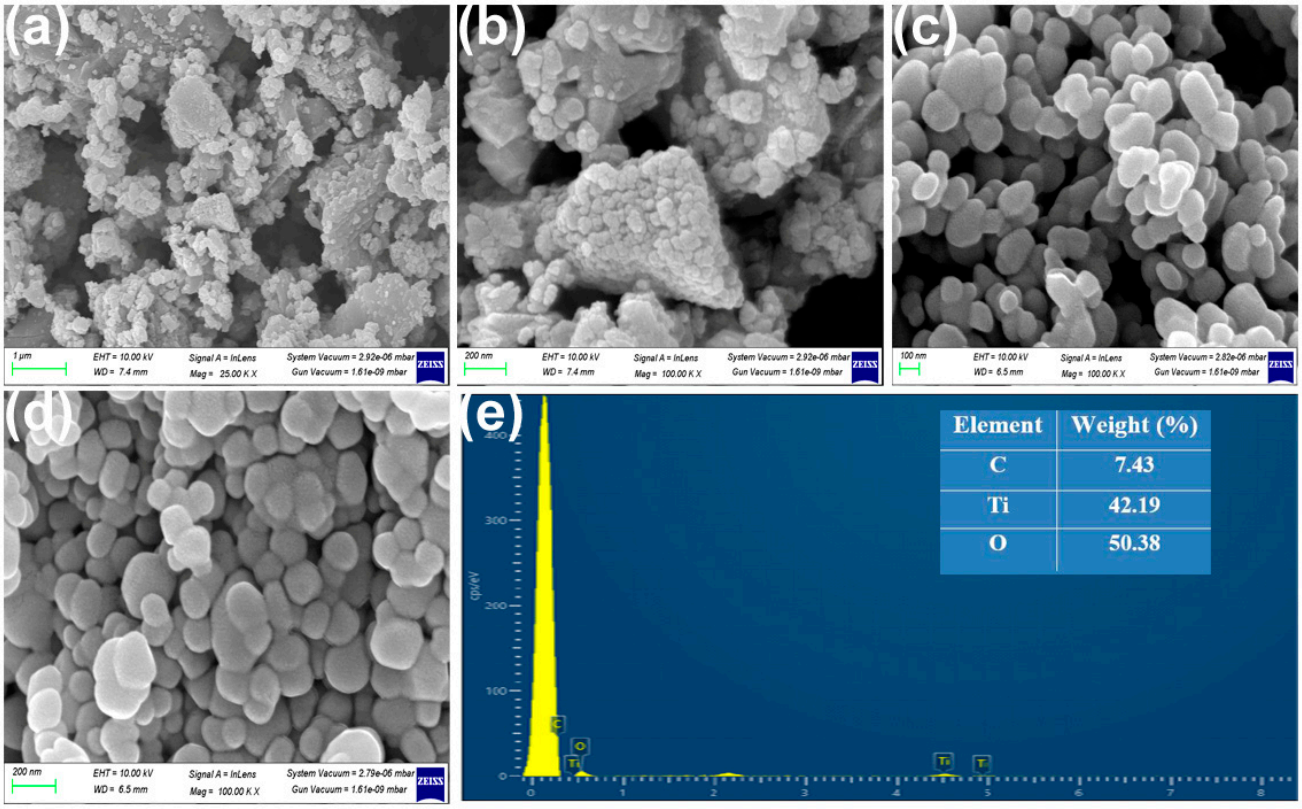

Figure 4. SEM images (**a**,**b**) of TiO_2, AC/TiO_2 nanoparticles (**c**,**d**) and EDX spectrum (**e**) of AC/TiO_2 nanoparticles.

The TEM images of AC/TiO_2 nanoparticles are displayed in Figure 5a,b. Figure 5a revealed that AC/TiO_2 nanoparticles are spherical in shape with dark spotted surfaces. Dark spotted surfaces indicated activated carbon doping on the TiO_2 nanoparticles. The TEM particle size of AC/TiO_2 nanoparticles is 22 nm. The hetero-compounds of activated carbon-doped titanium dioxide nanoparticles formed the improved morphology. The polycrystalline and obtained AC/TiO_2 nanoparticles' structural information was ensured by the SAED pattern of AC/TiO_2 nanoparticles, as shown in Figure 5b. The obtained particle sizes are well matched with the XRD crystallite size and SEM particle size. The spherical nanoparticles have large surface areas. The surface enhancement of nanoparticles simply strikes the organic pollutants or bacterial system and induces the charge carrier's productivity [55–57]. The spherical nanoparticles demonstrated an improved catalytic activity compared to other shaped nanoparticles.

3.5. XPS Analysis

The chemical composition and the valency of the synthesised AC/TiO_2 nanoparticles were determined from X-ray photoelectron spectroscopy. The XPS spectrum consists of wide Ti-2p, O-1s, and C-1s spectra for AC/TiO_2 nanoparticles, representing activated carbon, titanium, and oxygen, as shown in Figure 6. The Ti-2p spectrum is associated with oxygen and activated carbon, increasing the bonding between the synthesised nanoparticles. The Ti-2p spectrum is located at 458.6 eV (Ti-2p 3/2) and 466 eV (Ti-2p 1/2). The lattice oxygen spectrum is exhibited at 531 and 533 eV for O-1s, and their association in C=O and O-C=O is derived from activated carbon and plant extract. Their inclusion over the lattice oxygen stabilised the Ti^{4+} valency and improved the degradation of the organic dyestuffs. The activated carbon spectrum is located at 235 eV and represents the C-1s elements, which indicates the formation of activated carbon-doped TiO_2 nanoparticles. When doping the TiO_2 nanoparticles, activated carbon emanates the strongest binding between them. The

constructed results of Ti-2p, O-1s, and C-1s demonstrate the potential of their binding energy and the degradation potential of the AC/TiO_2 nanoparticles.

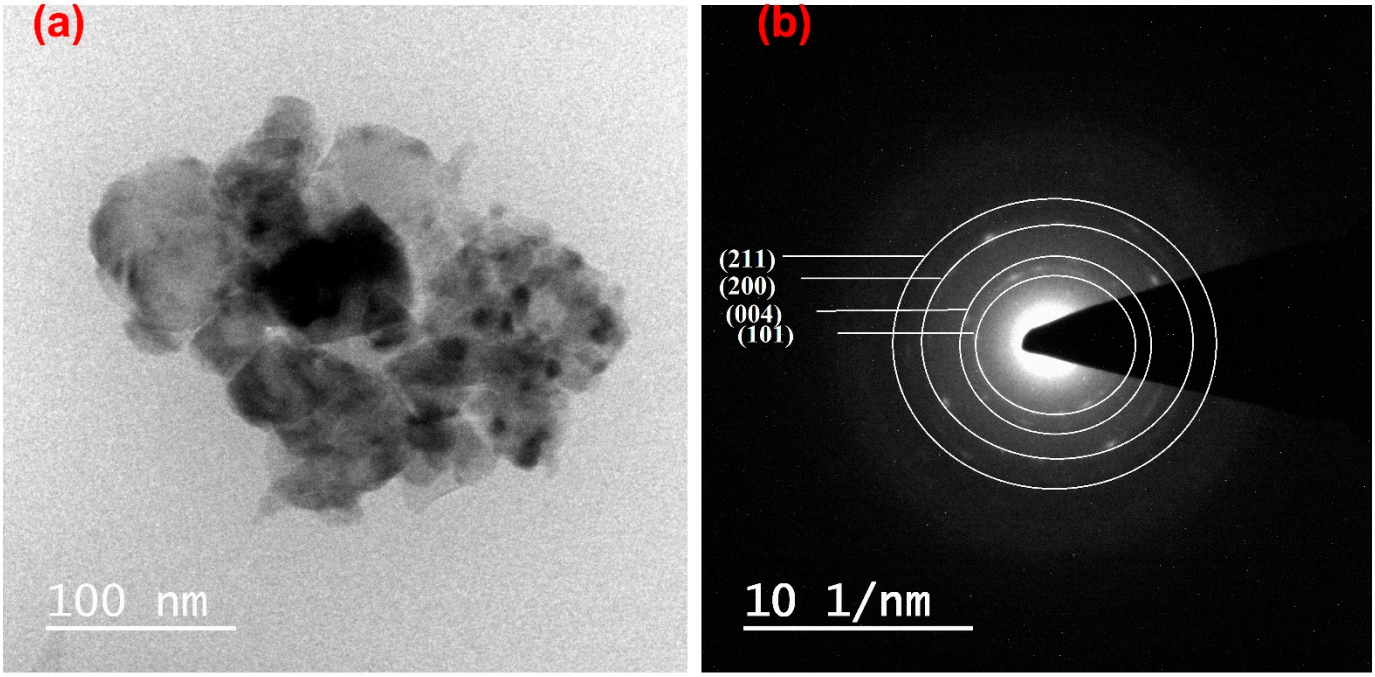

Figure 5. TEM image and SAED pattern (**a**,**b**) of AC/TiO_2 nanoparticles.

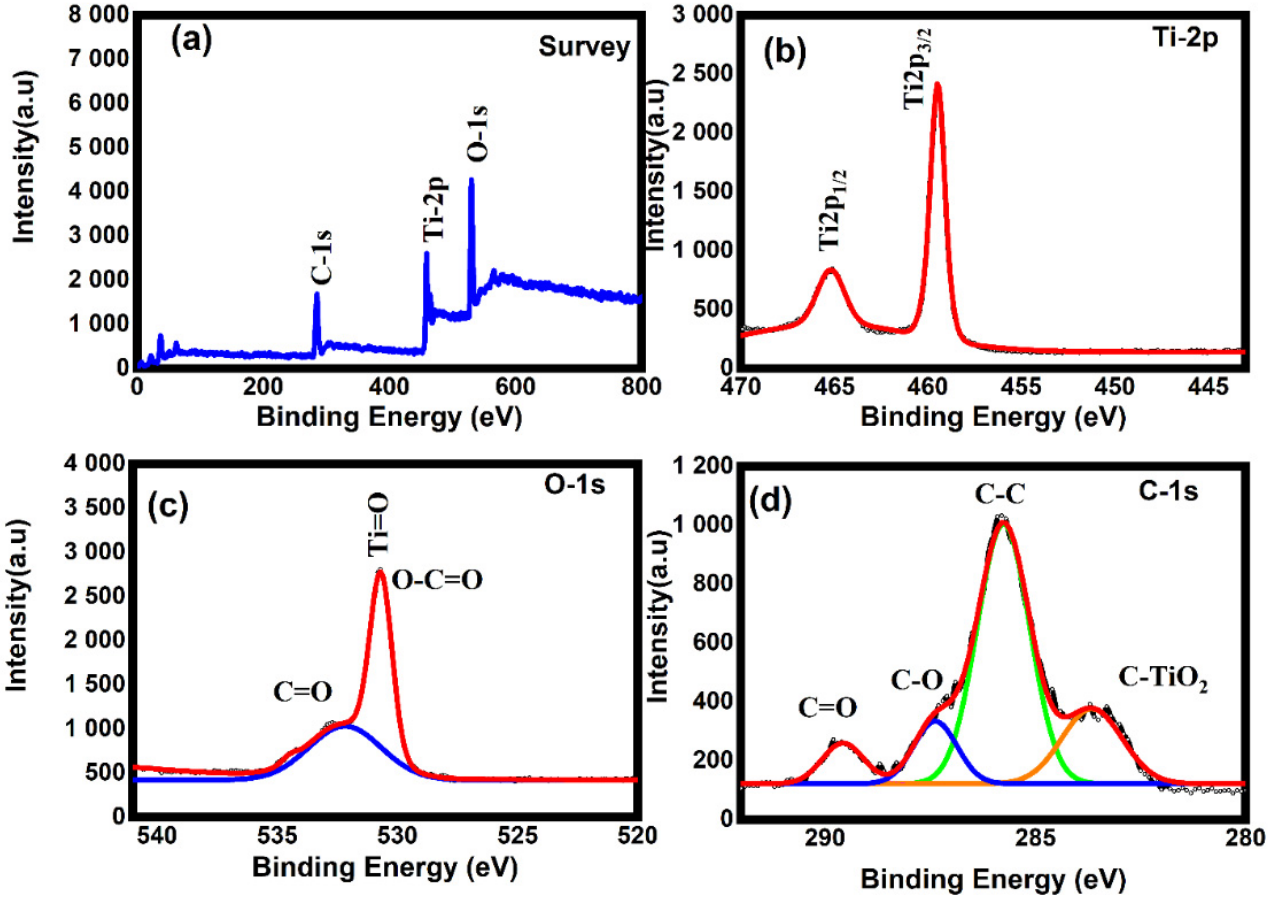

Figure 6. XPS images: wide (**a**), Ti-2 p (**b**), O-1s (**c**), and C-1s (**d**) of AC/TiO_2 nanoparticles.

3.6. Antibacterial Activity

The synthesised pure AC, plant extract, TiO_2, and AC/TiO_2 nanoparticles were examined against *S. aureus* (G-Positive) and *E. coli* (G-Negative) bacterial strains. The obtained bacterial results of the synthesised nanoparticles are displayed in Figures 7 and 8. The AC and plant extract (zapota) bacterial activities act as a standard antibacterial module, and it was compared with pure TiO_2 and AC/TiO_2 nanoparticles. The zone of inhibitions was evident by the inactivation of bacterial strains. Anatase TiO_2 nanoparticles revealed the highest activity in *E. coli* (G-Negative) bacterial strains compared to *S. aureus* (G-Positive) bacterial strains. The wide bandgap and extended recombination process formulated radical activity, which enhanced biological deactivation [58–60] as the activated carbon-doped titanium dioxide nanoparticles exhibited higher activity in *E. coli* than in *S. aureus*. The presented zone of inhibitions is based on the dosage-dependent manner, and their dissolution rate decides the bacterial dissociations. The antibacterial activity is AC < plant extract < TiO_2 < AC/TiO_2 nanoparticles. Every action is based on some procedure and protocol of the event. The bacterial inactivation mechanism is displayed in Figure 9. The entry of nanoparticles attacks the cell wall, and their strength disrupts the cell wall bonding. The leakage of the cell wall permits the entry of nanoparticles into the bacterial domain, which affects electron chain communications. The miscommunications in the cell system stop DNA and protein production, which affects the cell–nutrient system. A nutrient-free cell system gradually expresses its inactivation. Regarding the obtained findings, activated carbon-doped titanium dioxide nanoparticles improved their bio-sorption nature, and it is highly advisable to use bio-medical development-related devices [60–62].

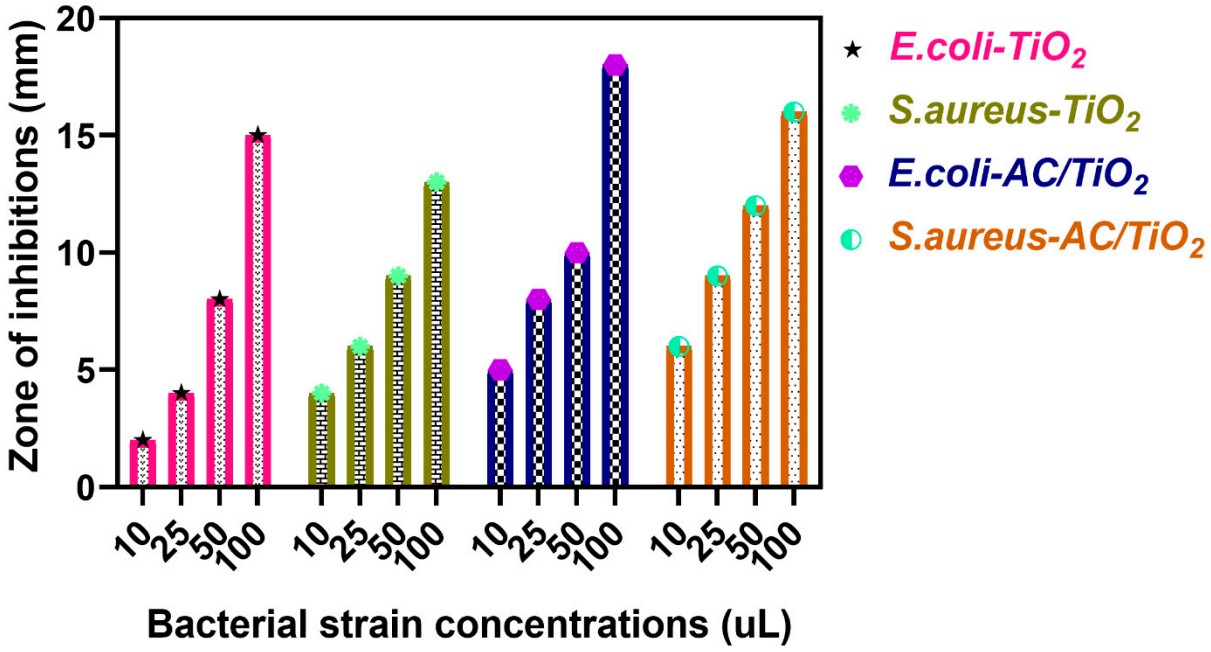

Figure 7. Zone of inhibitions of TiO_2 and AC/TiO_2 nanoparticles against various pathogens.

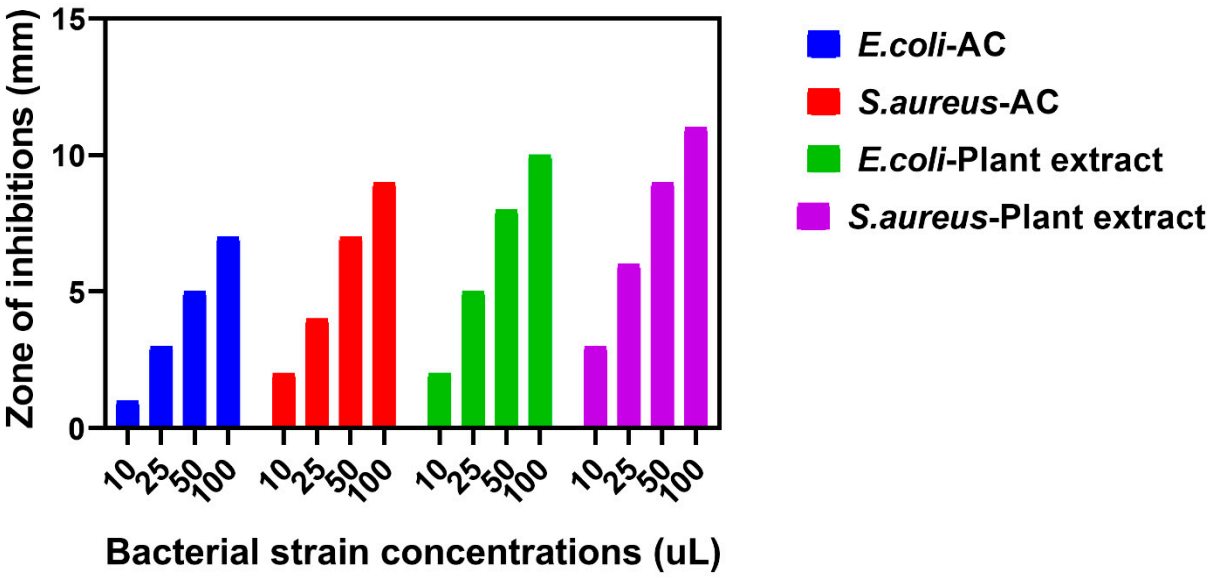

Figure 8. Zone of inhibitions of AC and plant extract against various pathogens.

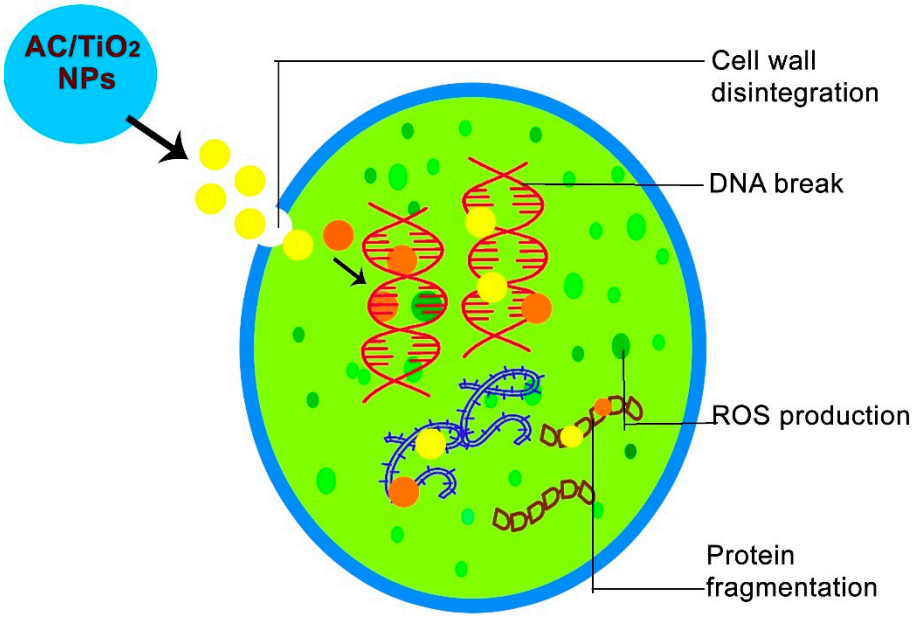

Figure 9. Antibacterial activity mechanism.

3.7. Photocatalytic Activity

The pure AC, TiO_2, and AC/TiO_2 nanoparticles' degradation efficiencies were determined from Rh-B dye under visible light irradiation. The organic pollutants are very noxious compounds and non-degradable and produce contagious diseases, which can be remediated using a nano-photocatalyst. Activated carbon (AC) degradation is 55% due to their active sites on the activated carbon surfaces. Pure TiO_2 nanoparticles decreased absorbance under light irradiation with respect to time. At 30 min intervals, pure TiO_2 nanoparticles showed a 73% degradation efficiency, and their values are presented in Figure 10a. The activated carbon doping to the anatase phase increased the adsorption behaviour and decreased the dye intensity from initial dye concentrations. The decreased absorbance determined the dissociation of dye molecules. The dye molecule fragments increased due to the microporous nature of activated carbon. At 30 min intervals, activated carbon-doped titanium dioxide exposed the 91% dye degradation. Anatase phase TiO_2 coupled with mesoporous/microporous activated carbon exhibited enhanced degradation

activity compared to pure TiO_2 nanoparticles. The C/C_0 spectrum demonstrated the degradation rate of pure TiO_2 and AC/TiO_2 nanoparticles, as shown in Figure 10c. The rate of degradation evaluation using pseudo-first-order kinetics and their calculated values are displayed in Figure 10c.

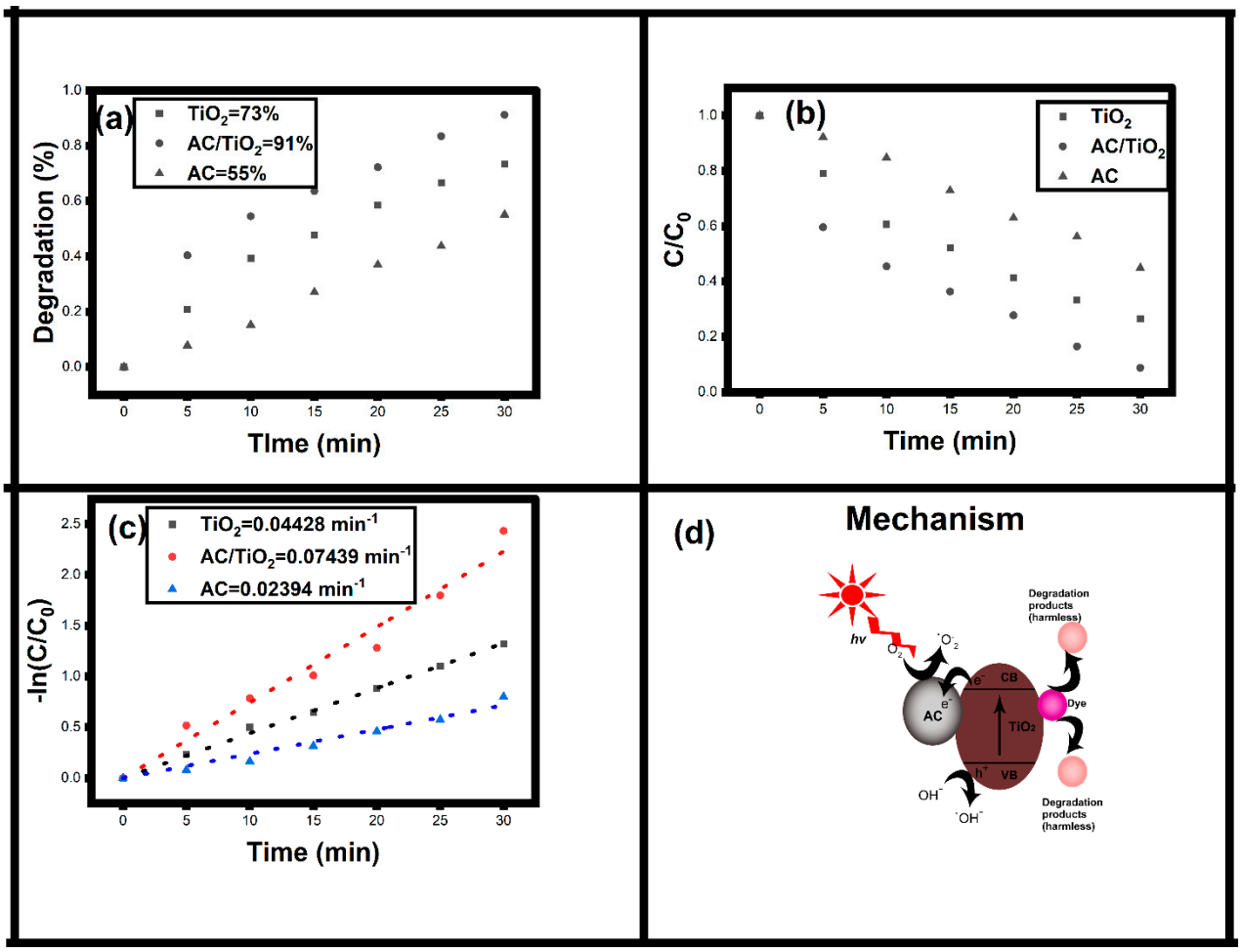

Figure 10. Photocatalytic degradation efficiency (**a**); C/C_0 (**b**); $-\ln(C/C_0)$ (**c**); and mechanism of AC, TiO_2 and AC/TiO_2 nanoparticles (**d**).

Comparatively, anatase TiO_2 nanoparticles revealed minimal degradation activity for 30 min (73%) compared to AC/TiO_2 nanoparticles (91%), confirming the high number of productions. The wide bandgap photocatalyst does not give better adsorption in visible light regions, which is overcome by doping of activated carbon. The photocatalytic mechanism of AC/TiO_2 nanoparticles is presented in Figure 10d, and their steps are as follows:

$$\mathbf{AC/TiO_2 + h\nu \rightarrow e^- (C.B) + h^+ (V.B)} \quad (1)$$

$$\mathbf{(H^+ + OH^-) + h^+ \rightarrow H^+ + {\cdot}OH} \quad (2)$$

$$\mathbf{O_2 + e^- \rightarrow O_2{}^- + H^+ + OH^- \rightarrow HO{\cdot}_2 + {}^-OH} \quad (3)$$

$$\mathbf{HO{\cdot}_2 + {}^-OH + h^+ \rightarrow {\cdot}OH} \quad (4)$$

$$\mathbf{Rh\text{-}B + {\cdot}OH \text{ and } O_2{}^{\cdot -} \rightarrow CO_2 + H_2O + \textit{by-products}} \quad (5)$$

The formation of activated carbon and titanium dioxide nanoparticles is based on the work functions. The excited electrons are transferred from lower work functional material to higher work function materials which establish the Schottky barrier. The light entry increased

the formation of e–h pairs [63,64]. The activated carbon reduced the bandgap and suppressed recombination, allowing excited electrons to move from the valence to the conduction bands. The free holes in the conduction band were engaged with the excited electrons [65,66]. This process is delayed by the doping of activated carbon. Furthermore, the deduction of recombination generated superoxide radicals and hydroxyl radicals. The above-mentioned productions help to convert the dye compounds to small noxious-free molecules. The photocatalytic degradation is influenced by holes and superoxides, and free radicals. Moreover, it can be responsible for efficient catalytic activity. The quenching experiment is displayed in Figure 11. The without-quenchers degradation percentage is 91%, and it can compare with holes, superoxides, and hydroxide suppression values. The figure presents the suppression values of IPA < BQ < TEOA for hydroxide < superoxides < holes, respectively. The holes' degradation endurance is better than the hydroxide and superoxide degradation efficiency, and their association with the photocatalyst improved the photocatalytic dye degradation activity. Based on the obtained findings, AC/TiO_2 nanoparticles demonstrated a high absorption capability and enriched the degradations.

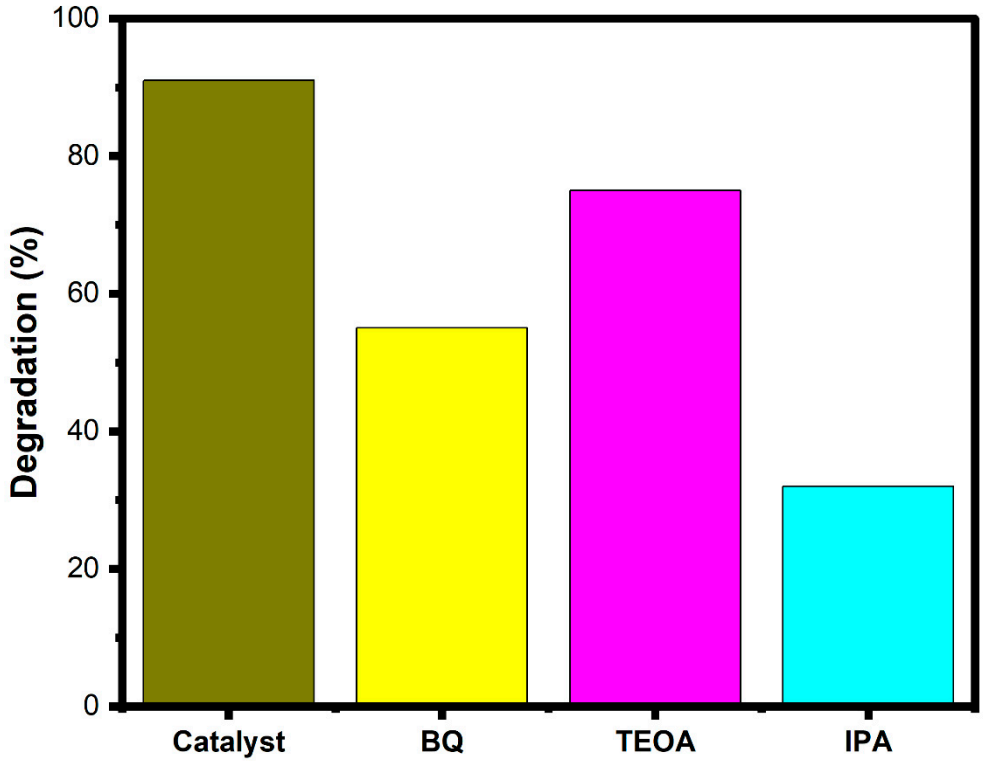

Figure 11. Quenching experiment.

4. Conclusions

The zapota leaf extract was used to prepare activated carbon doping titanium dioxide nanoparticles. The production of nanophase particles in a sustainable way reduced environmental risk and encouraged green calmness in the environment. The heterogeneous photocatalytic material of activated carbon-doped titanium dioxide nanoparticles entered/modified the TiO_2 lattice system and assisted the lattice distortions and reduction in the bandgap, enhanced the surface morphology, and created C-Ti-O formations. The activated carbon entry increased the visible light adsorption and generated the super oxide ions and hydroxyl radical on the surfaces. Reduced e–h pairs and carrier migrations increased the photocatalytic activity against Rh-B dye in AC/TiO_2 (91%) compared to TiO_2 (73%) nanoparticles. The bacterial investigation of *S. aureus* and *E. coli* against TiO_2 and AC/TiO_2 nanoparticles established the bacterial denaturation of the nanoparticles. *E. coli* bacteria are more active than *S. aureus* in the bactericidal activity of TiO_2 and AC/TiO_2 nanoparticles. Furthermore, according to the results of the characterization, TiO_2

and AC/TiO2 nanoparticles are more sensitive to all types of bacterial strains. Therefore, TiO_2 and AC/TiO_2 nanoparticles are potentially applicable for wastewater remediation development-related applications.

Author Contributions: Conceptualization, C.P. and S.K.; methodology, C.P.; software, M.A.I.; validation, C.P., S.K. and S.M.W.; formal analysis, C.P.; investigation, C.P.; re-sources, M.R.S., S.M.W. and W.-C.L.; data curation, S.K.; writing—original draft preparation, C.P.; writing—review and editing, C.P.; visualization, C.P.; supervision, C.P.; project administration, C.P.; funding acquisition, S.M.W. All authors have read and agreed to the published version of the manuscript.

Funding: The authors are grateful to the Researchers Supporting Project No. (RSP-2021/326), King Saud University, Riyadh, Saudi Arabia.

Data Availability Statement: All research data are associated with the manuscript.

Conflicts of Interest: The author has no conflict of interest.

References

1. Filho, W.L.; Totin, E.; Franke, J.A.; Andrew, S.M.; Abubakar, I.R.; Azadi, H.; Nunn, P.D.; Ouweneel, B.; Williams, P.A.; Simpson, N.P. Understanding responses to climate-related water scarcity in Africa. *Sci. Total Environ.* **2021**, *806*, 150420. [CrossRef] [PubMed]
2. Rafiei-Sardooi, E.; Azareh, A.; Shooshtari, S.J.; Parteli, E.J. Long-term assessment of land-use and climate change on water scarcity in an arid basin in Iran. *Ecol. Model.* **2022**, *467*, 109934. [CrossRef]
3. Aguilar, F.X.; Hendrawan, D.; Cai, Z.; Roshetko, J.M.; Stallmann, J. Smallholder farmer resilience to water scarcity. *Environ. Dev. Sustain.* **2021**, *24*, 2543–2576. [CrossRef]
4. Luukkonen, T.; Pehkonen, S.O. Peracids in water treatment: A critical review. *Crit. Rev. Environ. Sci. Technol.* **2017**, *47*, 1–39. [CrossRef]
5. Zobeidi, T.; Yaghoubi, J.; Yazdanpanah, M. Developing a paradigm model for the analysis of farmers' adaptation to water scarcity. *Environ. Dev. Sustain.* **2021**, *24*, 5400–5425. [CrossRef]
6. Zulu, N.N. Water Scarcity and Household Food Security: A Case of Ulundi Local Municipality in KwaZulu-Natal, South Africa. In *Handbook of Research on Resource Management and the Struggle for Water Sustainability in Africa*; IGI Global: Hershey, PA, USA, 2022; pp. 127–148.
7. Mir, R.; Azizyan, G.; Massah, A.; Gohari, A. Fossil water: Last resort to resolve long-standing water scarcity? *Agric. Water Manag.* **2021**, *261*, 107358. [CrossRef]
8. Zaheer, S.; Ahsan, S.; Ahmed, M.; Ahmed, A. An Empirical Analysis to Assess Climate Change and Its Effects on Water Scarcity Through Participatory Rural Apprasial (PRA) Approach in Chirirbandar Upazila, Dinajpur. In *Climate Change and Water Security*; Springer: Singapore, 2021; pp. 13–26.
9. Abd-Elaty, I.; Kuriqi, A.; El Shahawy, A. Environmental rethinking of wastewater drains to manage environmental pollution and alleviate water scarcity. *Nat. Hazards* **2021**, *110*, 2353–2380. [CrossRef]
10. Ahmed, Z.; Alam, R.; Ahmed, M.N.Q.; Ambinakudige, S.; Almazroui, M.; Islam, M.N.; Chowdhury, P.; Kabir, M.N.; Mahmud, S. Does anthropogenic upstream water withdrawal impact on downstream land use and livelihood changes of Teesta transboundary river basin in Bangladesh? *Environ. Monit. Assess.* **2022**, *194*, 59. [CrossRef]
11. Ji, B. Towards environment-sustainable wastewater treatment and reclamation by the non-aerated microalgal-bacterial granular sludge process: Recent advances and future directions. *Sci. Total Environ.* **2021**, *806*, 150707. [CrossRef]
12. Baskar, A.V.; Bolan, N.; Hoang, S.A.; Sooriyakumar, P.; Kumar, M.; Singh, L.; Jasemizad, T.; Padhye, L.P.; Singh, G.; Vinu, A.; et al. Recovery, regeneration and sustainable management of spent adsorbents from wastewater treatment streams: A review. *Sci. Total Environ.* **2022**, *822*, 153555. [CrossRef]
13. Danish, M.S.S.; Estrella-Pajulas, L.L.; Alemaida, I.M.; Grilli, M.L.; Mikhaylov, A.; Senjyu, T. Green synthesis of silver oxide nanoparticles for photocatalytic environmental remediation and biomedical applications. *Metals* **2022**, *12*, 769. [CrossRef]
14. Patil, S.P.; Chaudhari, R.Y.; Nemade, M.S. Azadirachta indica leaves mediated green synthesis of metal oxide nanoparticles: A review. *Talanta Open* **2022**, *5*, 100083. [CrossRef]
15. Chani, M.T.S.; Khan, S.B.; Rahman, M.M.; Kamal, T.; Asiri, A.M. Sunlight assisted photocatalytic dye degradation using zinc and iron based mixed metal-oxides nanopowders. *J. King Saud Univ. Sci.* **2022**, *34*, 101841. [CrossRef]
16. Singh, A.R.; Dhumal, P.S.; Bhakare, M.A.; Lokhande, K.D.; Bondarde, M.P.; Some, S. In-Situ synthesis of metal oxide and polymer decorated activated carbon-based photocatalyst for organic pollutants degradation. *Sep. Purif. Technol.* **2022**, *286*, 120380. [CrossRef]
17. Xiang, D.; Lu, S.; Ma, Y.; Zhao, L. Synergistic Photocatalysis-Fenton Reaction of Flower-shaped CeO_2/Fe_3O_4 Magnetic Catalyst for Decolorization of High Concentration Congo Red Dye. *Colloids Surf. A Physicochem. Eng. Asp.* **2022**, *647*, 129021. [CrossRef]
18. Gnanasekaran, L.; Rajendran, S.; Kumar, P.S.; Priya, A.; Gracia, F.; Habila, M.A.; Saravanakumar, K. Visible light stimulated binary nanostructure and defect enriched TiO_2-SnO_2 for photocatalysis and antibacterial activity. *Mater. Lett.* **2022**, *316*, 131998. [CrossRef]

19. Sudhagar, S.; Kumar, S.S.; Premkumar, I.J.; Vijayan, V.; Venkatesh, R.; Rajkumar, S.; Singh, M. UV-and visible-light-driven TiO_2/La_2O_3 and TiO_2/Al_2O_3 nanocatalysts: Synthesis and enhanced photocatalytic activity. *Appl. Phys. A* **2022**, *128*, 282. [CrossRef]
20. Wannapop, S.; Khawsaad, A.; Supanpong, A.; Janorat, Y.; Chuminjak, Y.; Tuantranont, A.; Phuruangrat, A.; Thongtem, T.; Thongtem, S.; Somdee, A. Photocatalytic study of metal oxide enhanced ZnO synthesized by a one-step cyclic-microwave method: The role of the pn heterostructure. *Inorg. Chem. Commun.* **2022**, *138*, 109210. [CrossRef]
21. Wang, X.; Cheng, H.; Ye, G.; Fan, J.; Yao, F.; Wang, Y.; Jiao, Y.; Zhu, W.; Huang, H.; Ye, D. Key factors and primary modification methods of activated carbon and their application in adsorption of carbon-based gases: A review. *Chemosphere* **2021**, *287*, 131995. [CrossRef]
22. Gayathiri, M.; Pulingam, T.; Lee, K.; Sudesh, K. Activated carbon from biomass waste precursors: Factors affecting production and adsorption mechanism. *Chemosphere* **2022**, *294*, 133764. [CrossRef]
23. Shen, Z.; Xing, X.; Wang, S.; Lv, M.; Li, J.; Li, T. Effect of K-modified blue coke-based activated carbon on low temperature catalytic performance of supported Mn–Ce/activated carbon. *ACS Omega* **2022**, *7*, 8798–8807. [CrossRef]
24. Yunus, Z.M.; Yashni, G.; Al-Gheethi, A.; Othman, N.; Hamdan, R.; Ruslan, N.N. Advanced methods for activated carbon from agriculture wastes; a comprehensive review. *Int. J. Environ. Anal. Chem.* **2020**, *102*, 134–158. [CrossRef]
25. Karimi-Maleh, H.; Karaman, C.; Karaman, O.; Karimi, F.; Vasseghian, Y.; Fu, L.; Baghayeri, M.; Rouhi, J.; Kumar, P.S.; Show, P.L.; et al. Nanochemistry approach for the fabrication of Fe and N co-decorated biomass-derived activated carbon frameworks: A promising oxygen reduction reaction electrocatalyst in neutral media. *J. Nanostruct. Chem.* **2022**, *12*, 429–439. [CrossRef]
26. Kempisty, D.M.; Arevalo, E.; Spinelli, A.M.; Edeback, V.; Dickenson, E.R.V.; Husted, C.; Higgins, C.P.; Summers, R.S.; Knappe, D.R.U. Granular activated carbon adsorption of perfluoroalkyl acids from ground and surface water. *AWWA Water Sci.* **2022**, *4*, e1269. [CrossRef]
27. Lunagariya, J.; Chabhadiya, K.; Pathak, P.; Mashru, D. Application of Taguchi Method in Activated Carbon Adsorption Process of Phenol Removal from Ceramic Gasifier Wastewater. *Environ. Chall.* **2022**, *6*, 100450. [CrossRef]
28. Susanto, H.; Mulyanti, R.; Istirokhatun, T.; Widiasa, I.N. Treatment of saline domestic wastewater using nanofiltration membrane coupled with activated carbon adsorption. *Urban Water J.* **2021**, *19*, 62–73. [CrossRef]
29. Xue, H.; Wang, X.; Xu, Q.; Dhaouadi, F.; Sellaoui, L.; Seliem, M.K.; Lamine, A.B.; Belmabrouk, H.; Bajahzar, A.; Bonilla-Petriciolet, A.; et al. Adsorption of methylene blue from aqueous solution on activated carbons and composite prepared from an agricultural waste biomass: A comparative study by experimental and advanced modeling analysis. *Chem. Eng. J.* **2022**, *430*, 132801. [CrossRef]
30. Bhatnagar, A.; Hogland, W.; Marques, M.; Sillanpää, M. An overview of the modification methods of activated carbon for its water treatment applications. *Chem. Eng. J.* **2012**, *219*, 499–511. [CrossRef]
31. Li, H.; Liang, L.; Niu, X.; Zhang, D.; Fan, H.; Wang, K. Construction of a Bi_2 WO_6/TiO_2 heterojunction and its photocatalytic degradation performance. *N. J. Chem.* **2022**, *46*, 8185–8194. [CrossRef]
32. Salawu, M.A.; Ayobami, A.A.; Adebisi, A.; Ezike, S.C.; Saheed, Y.O.; Alabi, A.B. Characterization of eosin red and hibiscus sabdariffa-based dye-sensitized solar cells. *Opt. Mater.* **2022**, *127*, 112177. [CrossRef]
33. Wang, C.; Bai, L.; Zhao, F.; Bai, L. Activated carbon fibers derived from natural cattail fibers for supercapacitors. *Carbon Lett.* **2022**, *32*, 907–915. [CrossRef]
34. Bergna, D.; Varila, T.; Romar, H.; Lassi, U. Activated carbon from hydrolysis lignin: Effect of activation method on carbon properties. *Biomass Bioenergy* **2022**, *159*, 106387. [CrossRef]
35. Pan, R.; Martins, M.F.; Debenest, G. Optimization of oil production through ex-situ catalytic pyrolysis of waste polyethylene with activated carbon. *Energy* **2022**, *248*, 123514. [CrossRef]
36. Alkorbi, A.S.; Javed, H.M.A.; Hussain, S.; Latif, S.; Mahr, M.S.; Mustafa, M.S.; Alsaiari, R.; Alhemiary, N.A. Solar light-driven photocatalytic degradation of methyl blue by carbon-doped TiO_2 nanoparticles. *Opt. Mater.* **2022**, *127*, 112259. [CrossRef]
37. Thinkohkaew, K.; Piroonpan, T.; Jiraborvornpongsa, N.; Potiyaraj, P. Development of multifunctional polypropylene nonwoven fabric by radiation induced grafting of TiO_2 nanoparticles and trifluoroethyl methacrylate for protective textile applications. *Materialia* **2022**, *21*, 101355. [CrossRef]
38. Singh, S.; Maurya, I.C.; Tiwari, A.; Srivastava, P.; Bahadur, L. Green synthesis of TiO_2 nanoparticles using Citrus limon juice extract as a bio-capping agent for enhanced performance of dye-sensitized solar cells. *Surfaces Interfaces* **2021**, *28*, 101652. [CrossRef]
39. Karthika, C.; Sureshkumar, R.; Sajini, D.V.; Ashraf, G.M.; Rahman, H. 5-fluorouracil and curcumin with pectin coating as a treatment regimen for titanium dioxide with dimethylhydrazine-induced colon cancer model. *Environ. Sci. Pollut. Res.* **2022**, 1–14. [CrossRef]
40. Nabgan, W.; Nabgan, B.; Abdullah, T.A.T.; Ikram, M.; Jadhav, A.H.; Jalil, A.A.; Ali, M.W. Highly Active Biphasic Anatase-Rutile Ni-Pd/TNPs Nanocatalyst for the Reforming and Cracking Reactions of Microplastic Waste Dissolved in Phenol. *ACS Omega* **2022**, *7*, 3324–3340. [CrossRef]
41. Jimoh, A.; Akpeji, B.; Azeez, S.; Ayipo, Y.; Abdulsalam, Z.; Adebayo, Z.; Ajao, A.; Zakariyah, A.; Elemike, E. Biosynthesis of Ag and TiO_2 nanoparticles and the evaluation of their antibacterial activities. *Inorg. Chem. Commun.* **2022**, *141*, 109503. [CrossRef]

42. Arutanti, O.; Sari, A.L.; Kartikowati, C.W.; Sari, A.A.; Arif, A.F. Design and Application of Homogeneous-structured TiO_2/Activated Carbon Nanocomposite for Adsorption–Photocatalytic Degradation of MO. *Water Air Soil Pollut.* **2022**, *233*, 118. [CrossRef]
43. Boumeftah, A.; Belmokhtar, A.; Benyoucef, A. Novel hybrid materials based on poly (4, 4′-Diaminodiphenyl sulfone) and TiO2 nanoparticles: Synthesis, characterization, physical and electrochemical properties. *Res. Chem. Intermed.* **2022**, *48*, 1717–1731. [CrossRef]
44. Tian, Z.; Wang, S.; Wu, Y.; Yan, F.; Qin, S.; Yang, J.; Li, J.; Cui, Z. Fabrication of polymer@ TiO_2 NPs hybrid membrane based on covalent bonding and coordination and its mechanism of enhancing photocatalytic performance. *J. Alloys Compd.* **2022**, *910*, 164887. [CrossRef]
45. Andrade-Guel, M.; Cabello-Alvarado, C.; Avila-Orta, C.A.; Pérez-Alvarez, M.; Cadenas-Pliego, G.; Reyes-Rodríguez, P.Y.; Rios-González, L. Green Flame-Retardant Composites Based on PP/TiO_2/Lignin Obtained by Melt-Mixing Extrusion. *Polymers* **2022**, *14*, 1300. [CrossRef]
46. Dessai, S.; Ayyanar, M.; Amalraj, S.; Khanal, P.; Vijayakumar, S.; Gurav, N.; Rarokar, N.; Kalaskar, M.; Nadaf, S.; Gurav, S. Bioflavonoid mediated synthesis of TiO_2 nanoparticles: Characterization and their biomedical applications. *Mater. Lett.* **2022**, *311*, 131639. [CrossRef]
47. Min, Y.; Song, G.; Zhou, L.; Wang, X.; Liu, P.; Li, J. Silver@ mesoporous Anatase TiO_2 Core-Shell Nanoparticles and Their Application in Photocatalysis and SERS Sensing. *Coatings* **2022**, *12*, 64. [CrossRef]
48. Keshari, A.K.; Choudhary, P.; Shukla, V.K. Precursor induced evolution in single anatase phase synthesis of TiO_2 nanoparticles for water treatment and dye-sensitized solar cell. *Phys. B Condens. Matter* **2022**, *631*, 413716. [CrossRef]
49. Wei, M.; Li, Z.; Chen, P.; Sun, L.; Kang, S.; Dou, T.; Qu, Y.; Jing, L. N-Rich Doped Anatase TiO_2 with Smart Defect Engineering as Efficient Photocatalysts for Acetaldehyde Degradation. *Nanomaterials* **2022**, *12*, 1564. [CrossRef]
50. Lekesi, L.; Motaung, T.; Motloung, S.; Koao, L.; Malevu, T. Investigation on structural, morphological, and optical studies of multiphase titanium dioxide nanoparticles. *J. Mol. Struct.* **2021**, *1251*, 132014. [CrossRef]
51. Bringley, E.J.; Manuputty, M.Y.; Lindberg, C.S.; Leon, G.; Akroyd, J.; Kraft, M. Simulations of TiO_2 nanoparticles synthesised off-centreline in jet-wall stagnation flames. *J. Aerosol Sci.* **2022**, *162*, 105928. [CrossRef]
52. Fischer, D.K.; de Fraga, K.R.; Scheeren, C.W. Ionic liquid/TiO_2 nanoparticles doped with non-expensive metals: New active catalyst for phenol photodegradation. *RSC Adv.* **2022**, *12*, 2473–2484. [CrossRef]
53. Nelsonjoseph, L.; Vishnupriya, B.; Amsaveni, R.; Bharathi, D.; Thangabalu, S.; Rehna, P. Synthesis and characterization of silver nanoparticles using Acremonium borodinense and their anti-bacterial and hemolytic activity. *Biocatal. Agric. Biotechnol.* **2021**, *39*, 102222. [CrossRef]
54. Mohammad, N.H.; El-Sherbiny, G.M.; Hammad, A.A.; Askar, A.A.; El-Nour, S.A.A. Gamma-ray and sunlight-induced synthesis of silver nanoparticles using bacterial cellulose and cell-free filtrate produced by Komagataeibacter rhaeticus N1 MW322708 strain. *Cellulose* **2022**, *29*, 1791–1805. [CrossRef]
55. Shah, I.H.; Ashraf, M.; Sabir, I.A.; Manzoor, M.A.; Malik, M.S.; Gulzar, S.; Ashraf, F.; Iqbal, J.; Niu, Q.; Zhang, Y. Green synthesis and Characterization of Copper oxide nanoparticles using Calotropis procera leaf extract and their different biological potentials. *J. Mol. Struct.* **2022**, *1259*, 132696. [CrossRef]
56. Balachandar, R.; Navaneethan, R.; Biruntha, M.; Kumar, K.K.A.; Govarthanan, M.; Karmegam, N. Antibacterial activity of silver nanoparticles phytosynthesized from Glochidion candolleanum leaves. *Mater. Lett.* **2021**, *311*, 131572. [CrossRef]
57. Zheng, B.-D.; Ye, J.; Yang, Y.-C.; Huang, Y.-Y.; Xiao, M.-T. Self-healing polysaccharide-based injectable hydrogels with antibacterial activity for wound healing. *Carbohydr. Polym.* **2021**, *275*, 118770. [CrossRef]
58. Wang, Y.; Wang, X.; Li, L.; Wu, Y.; Yu, Q. An experimental and theoretical study on the photocatalytic antibacterial activity of boron-doped TiO_2 nanoparticles. *Ceram. Int.* **2021**, *48*, 604–614. [CrossRef]
59. Karthikeyan, K.; Chandraprabha, M.N.; Krishna, R.H.; Samrat, K.; Sakunthala, A.; Sasikumar, M. Optical and antibacterial activity of biogenic core-shell $ZnO^{@}$ TiO_2 nanoparticles. *J. Indian Chem. Soc.* **2022**, *99*, 100361. [CrossRef]
60. Alghamdi, Y.G.; Krishnakumar, B.; Malik, M.A.; Alhayyani, S. Design and Preparation of Biomass-Derived Activated Carbon Loaded TiO_2 Photocatalyst for Photocatalytic Degradation of Reactive Red 120 and Ofloxacin. *Polymers* **2022**, *14*, 880. [CrossRef]
61. Rostami, M.; Badiei, A.; Ganjali, M.R.; Rahimi-Nasrabadi, M.; Naddafi, M.; Karimi-Maleh, H. Nano-architectural design of TiO_2 for high performance photocatalytic degradation of organic pollutant: A review. *Environ. Res.* **2022**, *212*, 113347. [CrossRef]
62. Shoneye, A.; Chang, J.S.; Chong, M.N.; Tang, J. Recent progress in photocatalytic degradation of chlorinated phenols and reduction of heavy metal ions in water by TiO_2-based catalysts. *Int. Mater. Rev.* **2021**, *67*, 47–64. [CrossRef]
63. Govindaraju, S.; Arumugasamy, S.K.; Chellasamy, G.; Yun, K. Zn-MOF decorated bio activated carbon for photocatalytic degradation, oxygen evolution and reduction catalysis. *J. Hazard. Mater.* **2022**, *421*, 126720. [CrossRef] [PubMed]
64. Xu, W.; Jin, Y.; Ren, Y.; Li, J.; Wei, Z.; Ban, C.; Cai, H.; Chen, M. Synergy mechanism for TiO_2/activated carbon composite material: Photocatalytic degradation of methylene blue solution. *Can. J. Chem. Eng.* **2022**, *100*, 276–290. [CrossRef]
65. Erim, B.; Ciğeroğlu, Z.; Şahin, S.; Vasseghian, Y. Photocatalytic degradation of cefixime in aqueous solutions using functionalized SWCNT/ZnO/Fe_3O_4 under UV-A irradiation. *Chemosphere* **2022**, *291*, 132929. [CrossRef] [PubMed]
66. Long, X.; Feng, C.; Yang, S.; Ding, D.; Feng, J.; Liu, M.; Chen, Y.; Tan, J.; Peng, X.; Shi, J.; et al. Oxygen doped graphitic carbon nitride with regulatable local electron density and band structure for improved photocatalytic degradation of bisphenol A. *Chem. Eng. J.* **2022**, *435*, 134835. [CrossRef]